Evaluation of nuclear charge radii based on nuclear radii changes

C. Ma,[1] Y. Y. Zong,[1] Y. M. Zhao,[1,2,*] and A. Arima[1,3,†]

[1]*Shanghai Key Laboratory of Particle Physics and Cosmology, School of Physics and Astronomy, Shanghai Jiao Tong University, Shanghai 200240, China*

[2]*Collaborative Innovation Center of IFSA (CICIFSA), Shanghai Jiao Tong University, Shanghai 200240, China*

[3]*Musashi Gakuen, 1-26-1 Toyotamakami Nerima-ku, Tokyo 176-8533, Japan*

(Received 22 October 2020; revised 23 April 2021; accepted 1 June 2021; published 6 July 2021)

In this paper we study the neutron-number dependence of δR (difference of nuclear charge radii R for two nuclei of one isotope chain), based on which we suggest an empirical formula of δR, called the δR relations. The δR relations of a number of theoretical models are also investigated in this work. We demonstrate that the δR relations of this work are more competitive than the previously called δR_{in-jp} relations, with the virtue of simplicity and flexibility. By using this approach we tabulate our predicted results of 1647 nuclear charge radii which are experimentally unaccessible, within theoretical uncertainty below 0.03 fm.

DOI: 10.1103/PhysRevC.104.014303

I. INTRODUCTION

The charge radius is one of the most fundamental properties of nuclei. This quantity also provides an important fingerprint for exotic nuclear structures like nuclear halos and shape coexistence [1–6].

Experimentally, root-mean-squared (rms) charge radii (denoted by R and $R \equiv \langle r^2 \rangle^{1/2}$) of many nuclei have been measured by using radioactive ion beams and ultrahigh-sensitivity laser spectroscopy techniques [6–9]. In a recent experimental database (denoted as CR2013 here) [10,11], the charge radii of 957 nuclei have been self-consistently determined by evaluating experimental data with multiple techniques. Although the results for Re, Po, Rn, Fr, Ra, and Cm isotopes compiled in this database were actually extrapolated from a global fit, as shown by Eq. (8) in Ref. [10], a more reliable evaluation for these isotopes is expected to be accessible in the near future, because muonic x-ray data have recently been collected on Re isotopes [12] and an experimental program is ongoing to measure the muonic x rays in Ra and Cm as well. Furthermore, benefiting from progress recently achieved by laser spectroscopy, many mean-squared charge-radius changes (denoted by $\delta R^{(2)}$, and $\delta R^{(2)} \equiv \delta \langle r^2 \rangle$), which were not included in the CR2013 database, have also been precisely determined [13–21].

Theoretically, the charge radii R have been calculated by using either microscopical models [22–28], macroscopic-microscopic approaches [29–33], or phenomenological formulas [34–40]. We note that the charge radii of 884 nuclei are reproduced with the root-mean-squared deviation (RMSD hereafter) of 0.027 fm by using the Skyrme-Hartree-Fock-Bogoliubov (HFB31) model in Ref. [24]; the RMSD is 0.035 fm with proper consideration of the diffuseness parameter in the framework of the finite-range liquid-drop model (FRLDM) [31]; more recently, a four-parameter charge-radius formula present the RMSD of 0.022 fm by considering the shell corrections and deformations in the Weizsäcker-Skyrme (WS*) mass model [40].

In addition to these sophisticated theoretical efforts, local relations of charge radii have been studied in recent years [41–45]. These relations are demonstrated to be very accurate. The RMSD of the Garvey-Kelson (GK) relations for nuclear charge radii is 0.01 fm [41]; the so-called δR_{in-jp} relations yield a RMSD of 0.003 fm [45], if very light nuclei and a few regions which exhibit either sharp phase transitions or shape coexistence (to be explained in Sec. II of this paper) are excluded. If one predicts nuclear charge radii by successive extrapolations of these local relations, however, one would see that the accuracy of predicted results decreases quickly with the number of times for successive extrapolations, because both experimental uncertainties of employed data and theoretical uncertainties of local relations contribute to the uncertainties of predicted results [46,47]. An avenue to improve the local-relation-based predictions is to reduce the number of experimental data involved in each step of extrapolation while retaining high accuracies of local relations.

It is therefore the purpose of this paper to investigate local relations of nuclear charge radii R which involve *only two charge radii in the same isotopic chain*, and to study both the descriptive and predictive powers of these local relations of R by numerical experiments. We demonstrate that these relations work remarkably well for nuclei in medium and heavy mass regions.

This paper is organized as follows. In Sec. II, we investigate the differences between charge radii of two nuclei in the same isotope chain but with k-neutron difference, denoted as δR_k, and study these quantities extracted from an empirical formula or more sophisticated models. In Sec. III,

*Corresponding author: ymzhao@sjtu.edu.cn

†Deceased.

we construct formulas of nuclear charge radii in terms of our predicted δR_k, and study the predictive power of these formulas by numerical experiments of extrapolations. Finally, we summarize this paper in Sec. IV.

II. SYSTEMATICS OF RMS CHARGE RADII DIFFERENCE BETWEEN TWO ISOTOPES

A. Empirical description of δR_k

Let us denote the charge-radius difference of two nuclei with the same proton number Z but different neutron numbers, N and $N-k$, by $\delta R_k(N,Z)$:

$$\delta R_k(N,Z) \equiv R(N,Z) - R(N-k,Z), \tag{1}$$

where $R(N,Z)$ is the root-mean-squared charge radius of nucleus with N neutrons and Z protons. As protons are electrically charged while neutrons are electrically neutral, nuclear charge radius is expected to be highly relevant to the proton number of the nucleus and to be insensitive to its neutron number. Assuming a spherical shape and a uniform proton distribution, the charge radius of a nucleus was conjectured to be essentially proportional to $Z^{1/3}$ [34,35]; if this is the case, one has a very naive relation

$$\delta R_k(N,Z) = 0. \tag{2}$$

We first investigate this relation for $k=1$. By using the latest version of nuclear charge-radius database, CR2013 [10], we plot the values of δR_1 with $N > 8$ in the upper panel of Fig. 1. To guide the eyes, we also plot the average values of δR_1 with given neutron number by using solid curves in red, from which one easily discerns a very subtle odd-even feature for δR_1. The average of overall δR_1 extracted from the CR2013 database (with $N > 8$) is +0.0072 fm, plotted by using dashed lines in green in Fig. 1(a). We note that most δR_1 values are positive; and this is easily understandable, as the volume of atomic nuclei is expected to increase on average with neutron number. From Fig. 1(a), one sees that the magnitudes of δR_1 are below 0.02 fm in most cases; the RMSD of the $\delta R_1 = 0$ relation is 0.014 fm, which is considerably smaller than those of many sophisticated global models.

Although the simple relation $\delta R_k = 0$, i.e., Eq. (2), works reasonably well for $k=1$ case, it is less useful when in the cases with larger values of k. For example, we plot the values of δR_2 extracted from CR2013 database [11], versus the neutron number N, in Fig. 1(b). One sees that the deviations of δR_2 from 0 are much larger than those in the case of $k=1$, and the RMSD value of Eq. (2) with $k=2$ is 0.023 fm. Such large deviations of the $\delta R_k = 0$ relation are found to originate mainly from three mechanisms. The first is attributed to the average deviation of δR_k from 0, as shown in Fig. 1. Apparently,

$$\delta R_k(N,Z) = \sum_{i=0}^{k-1} \delta R_1(N-i,Z), \tag{3}$$

and one expects that the average value of R_k is approximately proportional to k. This is supported by the average deviation of the $\delta R_2 = 0$ relation, $\overline{\delta R_2} = 0.0146$ fm $\approx 2\overline{\delta R_1}$ fm ($\overline{\delta R_1} = 0.0072$ fm, as discussed above). The second mechanism is

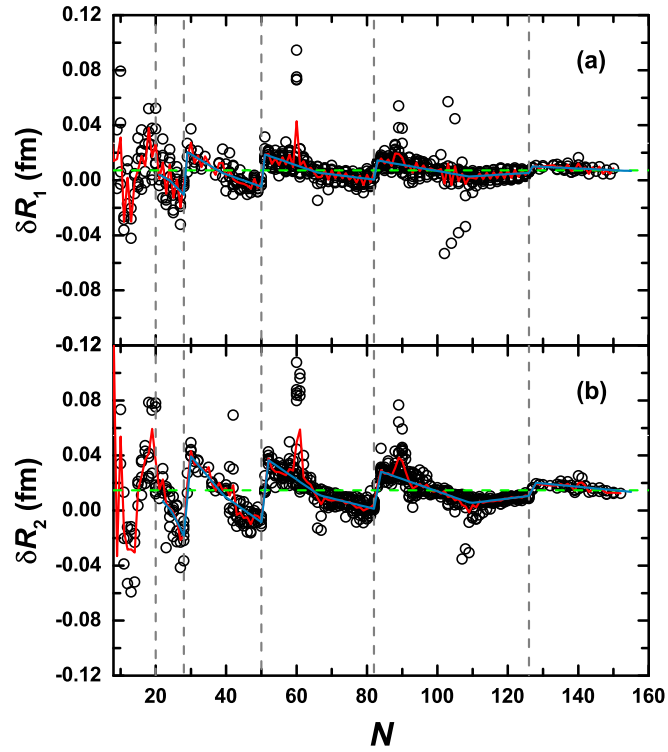

FIG. 1. Nuclear charge-radii changes, (a) δR_1 and (b) δR_2, extracted from the CR2013 database [10]. The curves in red correspond to the average values of δR_k ($k = 1, 2$) with neutron number N, and dashed lines in green represent the overall average of δR_k. δR_k of Eqs. (3) and (4) are plotted by using curves in blue.

the shell effect of neutrons. According to Fig. 1, the average deviation of δR_k increases vary sharply at the beginning of new neutron shells, and then decrease slowly throughout the shell; and this regular pattern leads to visible deviations of δR_1 from $\overline{\delta R_k}$ (dashed line in green). The third mechanism is related to the sudden onset of deformation or shape coexistence [6], which leads to anomalies of δR_k. In the CR2013 database [11], there are four such regions in terms of δR_1: (1) $N \leqslant 20$; (2) $N = 60$ and $37 \leqslant Z \leqslant 41$; (3) $88 \leqslant N \leqslant 90$ and $62 \leqslant Z \leqslant 67$; (4) $N \leqslant 108$ and $78 \leqslant Z \leqslant 79$, $N \leqslant 106$ and $Z = 80$. Such regions were also highlighted by the δR_{in-jp} relations. According to Eq. (3), these anomalous regions expand gradually with k.

In order to improve these δR_k relations, we introduce empirical corrections to describe the N dependence of δR_1 in average. Our empirical formula for δR_1 is

$$\delta R_1^{(\mathrm{emp})}(N,Z) = a(N-N_0) + b, \quad a = \begin{cases} a_1, & N < N_0, \\ a_2, & N \geqslant N_0, \end{cases} \tag{4}$$

where N_0 is generally set as neutron number at the half-filled neutron shell, except that $N_0 = 109$ for the $N = 82$–126 shell (rather than $N_0 = 104$); namely, we take $N_0 = 24$, 39, 66, 109, and 155. a_1, a_2, and b are parameters optimized by using the experimental values of δR_1 for each major shell, and are presented in Table I. $\delta R_k^{(\mathrm{emp})}$ with $k > 1$ are calculated by

TABLE I. Optimized parameters a_1, a_2, and b [see Eq. (4), in units of 10^{-3} fm] obtained by a χ^2 fitting to the δR_1 values extracted from the CR2013 database [10,11].

Parameter	$21 \leqslant N \leqslant 28$	$29 \leqslant N \leqslant 50$	$51 \leqslant N \leqslant 82$	$83 \leqslant N \leqslant 126$	$N \geqslant 127$
a_1 ($\times 10^{-3}$ fm)	−1.417	−1.520	−0.881	−0.449	−0.121
a_2 ($\times 10^{-3}$ fm)	−2.577	−0.899	−0.317	0.158	
b ($\times 10^{-3}$ fm)	−0.150	5.226	5.548	2.696	6.744

using Eq. (4) and the definition in Eq. (3). We note that, although these parameters are not optimized for $k > 1$ cases, we find they are close to those optimized individually for each k; and in this paper we assume unified values of a_1, a_2, and b for different k.

The δR_1 and δR_2 calculated by using Eq. (4) with parameters of Table I are plotted in Fig. 1 (solid curves in blue). One sees that the evolution of δR_1 and δR_2 is very well represented by Eq. (4). On the other hand, the shape transition or coexistence is not considered in Eq. (4), therefore in the discussions below we exclude those four regions involving anomalous δR_1. The deviations of calculated δR_1 and δR_2 (denoted by $\delta R_1^{(\mathrm{emp})}$ and $\delta R_2^{(\mathrm{emp})}$) from those extracted based on the CR2013 database (denoted by $\delta R_1^{(\mathrm{exp})}$ and $\delta R_2^{(\mathrm{exp})}$) are plotted in Fig. 2, where most of deviations are smaller than 0.02 fm. While the odd-even feature is discernible for δR_1, it is not seen for δR_2. The average deviations, $\overline{\delta R_k^{(\mathrm{emp})}}(N) - \overline{\delta R_k^{(\mathrm{exp})}}(N)$ with $k = 1$ and 2, are very close to 0, as shown by solid curves in red.

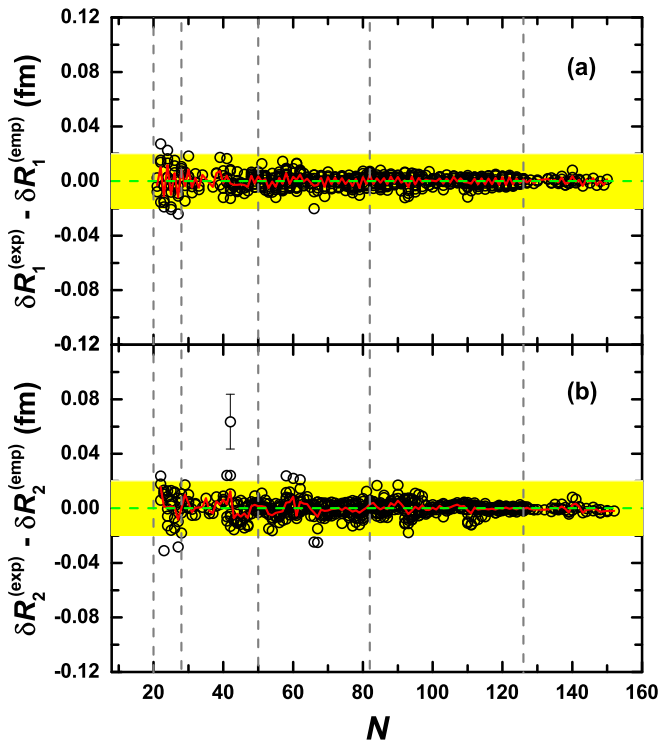

FIG. 2. Deviations of (a) δR_1 and (b) δR_2 based on Eqs. (3) and (4) from those extracted from the CR2013 database. The average deviations with given neutron number N is plotted by using curves in red, and the overall averages of δR_1 and δR_2 are plotted by using dashed lines in green. The vertical dashed lines correspond to neutron magic numbers.

With Eq. (4), the resultant RMSD of $\delta R_1^{(\mathrm{emp})}$ is 0.0050 fm, which is much smaller than the $\delta R_1 = 0$ relation for the same set of experimental data. Such improvement is even more striking for $k > 1$. By using Eqs. (3) and (4), the RMSD for δR_2 is 0.0063 fm, which is about one-third of that for the $\delta R_2 = 0$ relation. Yet, from the lower panel of Fig. 2 there is one result for which the deviation of δR_2 is very large at $N = 42$ corresponding to the $^{76}_{34}\mathrm{Se}_{42}$ nucleus, whose experimental uncertainty of $\delta R_2^{(\mathrm{exp})}$ is ~ 0.02 fm. However, the uncertainty of $\delta R_2^{(\mathrm{exp})}$ is sizably smaller than $|\delta R_2^{(\mathrm{emp})} - \delta R_2^{(\mathrm{exp})}|$. We note that $^{74}_{34}\mathrm{Se}_{40}$ is located at the region of phase transition. If we exclude this anomaly from evaluation, the resultant RMSD would be reduced from 0.0063 fm to 0.0058 fm.

B. δR_k based on theoretical models

As an alternative approach of Eqs. (3) and (4), in this subsection we study the nuclear charge radii based on a number of theoretical databases [24,26,28,40], which are described very briefly as follows. In Ref. [24], the self-energy effects are considered in the Hartree-Fork-Bogoliubov (HFB) model by adding a purely phenomenological density-gradient-dependent term in the pairing force; and by setting the symmetry coefficient as 31 MeV, one obtains the HFB-31 results. In Ref. [28], a comprehensive calculation is performed by using the spherical relativistic continuum Hartree-Bogoliubovc (RCHB) theory, with the relativistic density functional PC-PK1 [27] and consideration of the continuum effects. In Ref. [26], the relativistic mean field model plus a state-dependent BCS method (RMF + BCS) are employed to study the ground-state properties of all bound nuclei. In Ref. [40], a four-parameter formula is proposed to describe R by combining the shell corrections and deformations of nuclei given from the Weizsäcker-Skyrme (WS*) model. For convenience, we denote all results of these models by using a superscript "(th)".

In Fig. 3, $\delta R_1^{(\mathrm{th})}$ which are experimentally accessible in the CR2013 database are extracted from calculated R values of the above four theoretical models (denoted by HFB-31, RCHB, RMF + BCS, and WS*), and are plotted in panels (a)–(d). The average values of $\delta R_1^{(\mathrm{th})}$ with given N are plotted by solid lines in red, and the overall average values are plotted by dashed lines in green ($\sim$0.007 fm for all panels, close to that in Fig. 1). From this figure, one sees that the neutron shell effect on δR_1 is well reproduced by these models, except the RCHB model, whose $\delta R_1^{(\mathrm{th})}$ are less sensitive to neutron shells than that of $\delta R_1^{(\mathrm{exp})}$. As discussed in the last subsection, the experimental

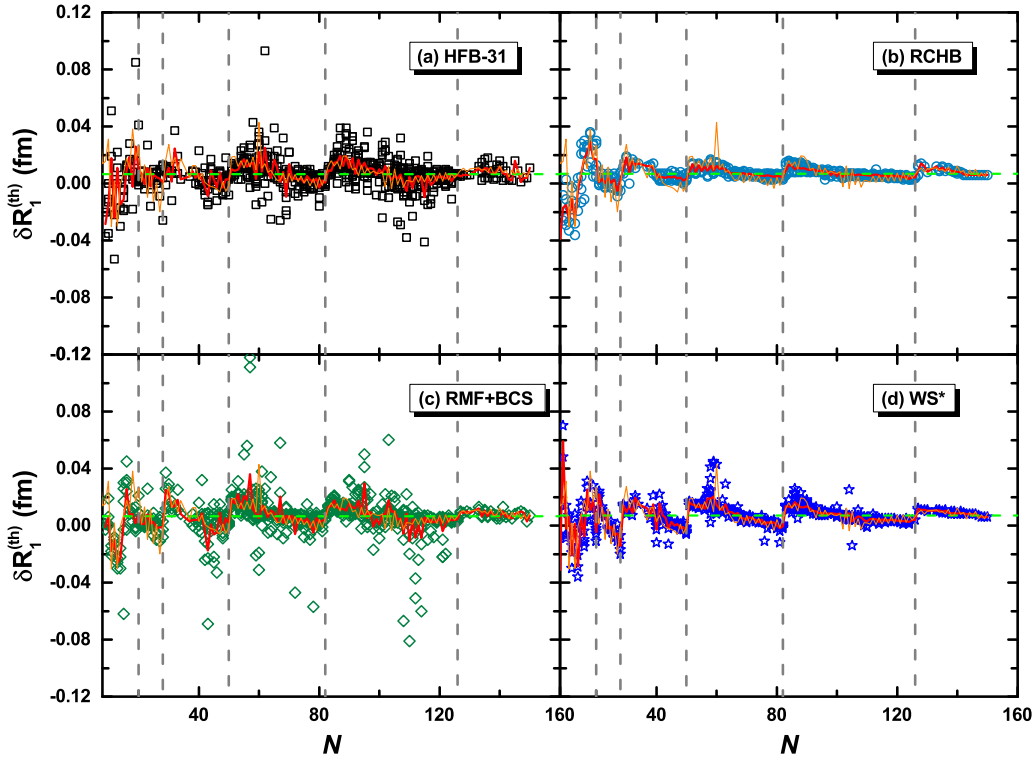

FIG. 3. δR_1 (in unit of fm, for those accessible in the CR2013 database) extracted from a few theoretical calculations: (a) HFB-31 [24], (b) RCHB [28], (c) RMF + BCS [26] and (4) WS* [40]. The curves in red correspond to the average values with given neutron number N, and dashed lines in green correspond to the overall average values of nuclei with $N > 8$. The average values of δR_1 based on the CR2013 database are plotted by using orange curves, for the sake of comparison and convenience, and the vertical dashed lines in grey correspond to neutron magic numbers.

δR_1 exhibits an odd-even feature. Unfortunately, the average of HFB-31- and RMF + BCS-based $\delta R_1^{(th)}$ does not exhibit such odd-even staggering in the right behavior; on the contrary, the "staggering" is sometimes opposite to that of $\delta R_1^{(exp)}$. Furthermore, for these two models, there are many large $\delta R_1^{(th)}$ that originate from shape transition and coexistence in the models; these will be discussed later. Therefore, the RMSD values of $\delta R_1^{(th)} - \delta R_1^{(exp)}$ from zero (0.0149 and 0.0161 fm, respectively) are considerably larger than those for the RCHB and WS* models (0.0107 and 0.0119 fm, respectively), as listed in the first row of Table II. For the sake of convenience, in the third row of Table II we list the RMSD values of the charge radii R for these four models, from their experimental values in the CR2013 database [10,11]. One sees that the RMSD of $\delta R_1^{(th)}$ is much smaller than that of $R^{(th)}$ for each of four models.

In the second rows of Table II, we present the RMSD values of $\delta R_1^{(th)}$ extracted by using these formulas and models, with exclusion of the four anomalous regions pointed out in Sec. II A, from corresponding δR_1 extracted from the CR2013 database. The RMSD of the δR_1 with this requirement is reduced from over 0.01 fm to 0.0057 and 0.0066 fm for the RCHB and WS* models, respectively. These RMSD values are also substantially smaller than the RMSD values of $R^{(th)}$ (see the fourth row of Table II), obtained by excluding the same set of anomalous regions.

TABLE II. Root-mean-square deviations (RMSD) of δR_1 and R extracted from databases of a few theoretical models (HFB-31 [24], RCHB [28], RMF+BCS [26], and WS* [40]), with respect to those of the CR2013 database [10,11]. The first and third rows correspond to the RMSD values of all nuclei accessible in the CR2013 database with $N > 8$, while those in the second and fourth rows are results with exclusion of the four anomalous regions pointed out in Sec. II A. $\mathcal{N}$ is the number of total data sets. For convenience of discussion, we also present here the results of Eq. (4) in the last column.

	$\mathcal{N}$	HFB-31	RCHB	RMF+BCS	WS*	Eq. (4)
	730	0.0149	0.0107	0.0161	0.0119	
δR_1	651	0.0105	0.0057	0.0130	0.0066	0.0050
	929	0.0272	0.0358	0.0350	0.0218	
R	828	0.0247	0.0332	0.0331	0.0199	

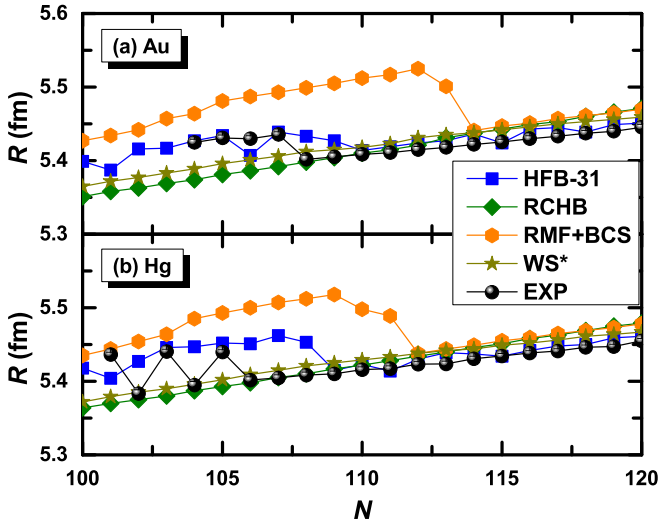

FIG. 4. Nuclear charge radii R for Au ($Z = 79$) and Hg ($Z = 80$) isotopes. Experimental R in the CR2013 database [10,11] are denoted by solid balls in black, and theoretical R calculated by the HFB-31 [24], RCHB [28], RMF + BCS [26], and WS* [40] models are shown in other colors.

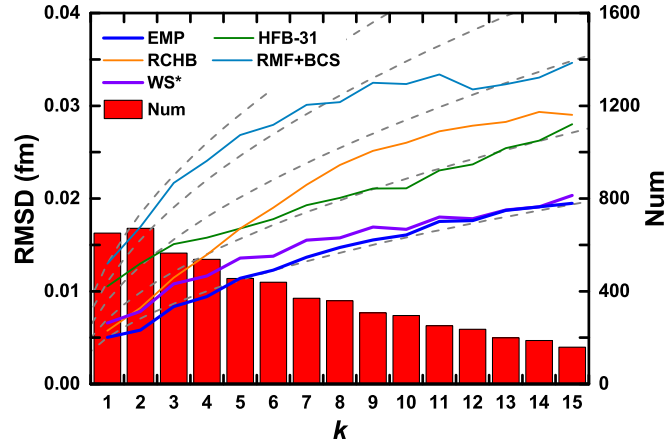

FIG. 5. RMSD values of theoretical δR_k from those of the CR2013 database [10,11]. Solid lines (in blue, green, orange, cyan, purple) correspond to δR_k based on our formula [denoted by "EMP"; see Eq. (4)], the HFB-31, RCHB, RMF + BCS, and WS* calculations, respectively. The histograms in red correspond to the number of δR_k versus k in the calculations. The dashed lines correspond to simple functions $0.005k^{1/2}$, $0.007k^{1/2}$, $0.009k^{1/2}$, $0.011k^{1/2}$, and $0.013k^{1/2}$ (in fm), which are used to guide eyes.

Before we go to the cases of $\delta R_k^{(\mathrm{th})}$ with $k > 1$, to be complete, it is informative to take a look at the agreement of our approach with experimental data for regions which were called "anomalous" in the above discussions. Here we exemplify these anomalies by using the Au and Hg isotopes. In Fig. 4, we plot the nuclear charge radii of these two isotope chains obtained by the HFB-31, RCHB, RMF + BCS, and WS* calculations as well as those compiled in the CR2013 databases. For Au isotopes, one sees an abrupt decrease of experimental charge radii at $N = 107$ and 108, indicating strongly prolate deformation in the ground states of these isotopes with $N \leqslant 107$ [6]. As for the Hg isotopes, a large odd-even staggering is clearly seen in experimental values of R when $N \leqslant 105$. None of these patterns are satisfactorily reproduced by these theoretical models, unfortunately, because the complex competition between prolate and oblate quasidegenerate states near the energy minima is highly sensitive to details of the effective interaction [21,48]. We also note that the RCHB and WS* calculated charge radii do not exhibit any anomalies here: in the RCHB calculation, deformation is not considered; and in the WS* model, the reason of this failure is warranted for further investigation, as the deformation parameters have been integrated in the formulations (see Eq. (1) in Ref. [40]).

Now let us discuss the $\delta R_k^{(\mathrm{th})}$ with $k > 1$. We extract $\delta R_k^{(\mathrm{th})}$ based on the HFB-31, RCHB, RMF + BCS, and WS* models, as well as those based on the Eqs. (3) and (4), and then investigate these $\delta R_k^{(\mathrm{th})}$ with exclusion of the four anomalous regions mentioned in Sec. II A. For given value of k, the RMSD values with respect to $\delta R_k^{(\mathrm{exp})}$ extracted from the CR2013 database are plotted in Fig. 5 for each set of models, with $k = 1$ to $k = 15$.

It is, first of all, interesting to discuss the k dependence of the RMSD values. If all $\delta R_1^{(\mathrm{th})} - \delta R_1^{(\mathrm{exp})}$ are statistically independent and Gaussian distributed with a width σ_1, the distribution width σ_k of δR_k will be given by ${\sigma_k}^2 = k{\sigma_1}^2$, namely, the RMSD values of δR_k relations are expected to be proportional to $k^{1/2}$. However, most σ_k results here do not agree with this pattern, as shown in Fig. 5. To guide the eyes, we plot in Fig. 5 simple functions $\sigma_1 k^{1/2}$, where σ_1 ranges from 0.005 to 0.013 fm with an interval of 0.002 fm, using dashed lines in grey. For $k = 1$, the RMSD of theoretical models discussed in this paper could be divided into two groups, one of which includes Eq. (4), RCHB and WS* models with the RMSD around 0.005 fm, and the other includes the HFB-31 and RMF + BCS models with the RMSD beyond 0.010 fm. One sees here that the results of Eq. (4) and WS* models approximately follow the $k^{1/2}$ pattern, while the RMSD of the RCHB model increases more rapidly than the $k^{1/2}$ pattern for $k > 4$. In the second group with $\sigma_1 \sim 0.01$ fm, however, the RMSD values based on the HFB-31 and RMF + BCS models increase more slowly than the $k^{1/2}$ pattern (although the RMSD values based on the RMF + BCS model follow this pattern for $k \leqslant 7$). The RMSD based on the HFB-31 model is even smaller than that based on the RCHB model for $k \geqslant 6$. One of main reasons that the RMSD values of δR_k based on the RCHB model increase most rapidly with k is the inappropriate description of evaluation of $\delta R_1^{(\mathrm{th})}$ with N: One sees from Fig. 3(b) that $\delta R_1^{(\mathrm{th})}$ decrease more slowly with k than $\delta R_1^{(\mathrm{exp})}$ does and the $\delta R_1^{(\mathrm{th})}$ for nuclei near the neutron shells are closer to the overall average value. This makes the $\delta R_1^{(\mathrm{th})} - \delta R_1^{(\mathrm{exp})}$ of nuclei in the first half neutron shell essentially negative and those in the second half shell essentially positive, i.e., they are statistically random but not with respect to zero.

From Fig. 5, one sees that the results of δR_k relations based on Eq. (4) and WS* models work best for $k \geqslant 2$. The RMSD of these two R_k relations are considerably smaller than those of the HFB-31 and RMF + BCS models for $k = 1$ and

increase more slowly than that of the RCHB model. It is also worthwhile to note that an odd-even feature is discernible in Fig. 5 for these two relations, with larger RMSD for odd k. This is actually expected, if one realizes that neither Eq. (4) nor the WS* model reproduce the odd-even staggering exhibited in the δR_k with odd k. unfortunately, this odd-even staggering of the RMSD versus k is too weak to be useful in applications.

III. PREDICTIVE POWER OF δR_k RELATIONS

In this section, we study predictive power of our δR_k relations by two numerical experiments, one of which is an extrapolation from earlier databases, the CR1999 [49] and CR2004 [50] databases, to the CR2013 database [10], and the other of which is to predict latest experimental results from the CR2013 database, for both nuclear charge radius R and the mean-squared charge-radius difference that is defined as

$$\delta R^2(N,Z) = R(N,Z)^2 - R(N^*,Z)^2, \tag{5}$$

where N^* is our so-called "reference" neutron number in this paper.

The procedure of our extrapolation is as follows. First, we extract values $\delta R_1^{(\mathrm{th})}$ for $N \geqslant 21$ based on various models including HFB-31, RCHB, RMF + BCS, and WS4* models, and $\delta R_1^{(\mathrm{emp})}$ based on Eq. (4) with parameters a_1, a_2, and b in Table I. Second, $\delta R_k^{(\mathrm{th})}$ are calculated by using its definition [see Eq. (3)] for $k = 2$–15. In doing so, we exclude the $\delta R_k^{(\mathrm{th})}$ of nuclei in the anomalous regions discussed in Sec. II A. Finally we make use of these $\delta R_k^{(\mathrm{th})}$, and obtain the prediction of nuclear charge radius by using the simple relations

$$R_k^{(\mathrm{pred})}(N,Z) = R^{(\mathrm{exp})}(N-k,Z) + \delta R_k^{(\mathrm{th})}(N,Z), \tag{6}$$

$$R_k^{(\mathrm{pred})}(N,Z) = R^{(\mathrm{exp})}(N+k,Z) - \delta R_k^{(\mathrm{th})}(N+k,Z), \tag{7}$$

where $R_k^{(\mathrm{pred})}(N,Z)$ is the predicted charge radius of a nucleus with N neutrons and Z protons, and $R^{(\mathrm{exp})}$ is the experimental charge radius. Equations (6) and (7) are the key relations in our extrapolations in this paper.

The theoretical uncertainty of $\delta R_k^{(\mathrm{th})}$, denoted by σ_k, is obtained by assuming that $\delta R_1^{(\mathrm{th})}$ are centered at zero and Gaussian distributed (although this assumption is not very good and thus yields relatively larger theoretical uncertainties of the δR_k relations). Therefore, our theoretical uncertainties of Eqs. (6)–(7), denoted by using $\sigma_k^{(\mathrm{pred})}(N,Z)$, are

$$\sigma_k^{(\mathrm{pred})}(N,Z) = \sqrt{\sigma^{(\mathrm{exp})2}(N-k,Z) + k\sigma_1{}^2}, \tag{8}$$

$$\sigma_k^{(\mathrm{pred})}(N,Z) = \sqrt{\sigma^{(\mathrm{exp})2}(N+k,Z) + k\sigma_1{}^2}, \tag{9}$$

where $\sigma^{(\mathrm{exp})}(N,Z)$ corresponds to the experimental uncertainty of $R^{(\mathrm{exp})}(N,Z)$, and σ_1 represents the theoretical uncertainty of $\delta R_1^{(\mathrm{th})}$, which is assumed to be 0.011, 0.005, 0.011, 0.006, and 0.005 fm for the HFB-31, RCHB, RMF + BCS, WS* models and the Eq. (4) formula. There are at most $2\times 15 = 30$ predictions for a given nucleus, and the $R_k^{(\mathrm{pred})}(N,Z)$ with the smallest theoretical uncertainty is adopted as our predicted value.

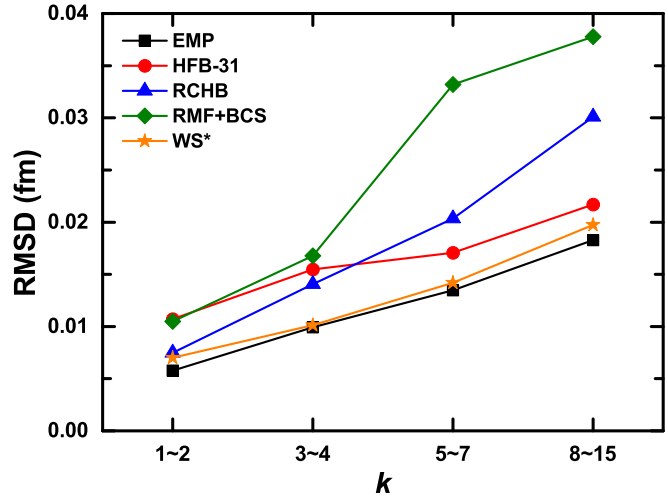

FIG. 6. RMSD (in units of fm) of our extrapolated charge radii, from the CR1999 database [49] to the CR2013 database [10,11], for k = 1–2, 3–4, 5–7, and 8–15.

Our first numerical experiment is to predict the results in the CR2013 databases [10,11] starting from the CR1999 database [49] in which there are in total 244 charge radii accessible for $N \geqslant 20$ (with exclusion of the four anomalous regions discussed above). By using Eqs. (6)–(7) and (8)–(9), we totally predict 464 nuclear charge radii which are not accessible in Ref. [49] but are compiled in Ref. [11]. For convenience of our discussion, these extrapolated results are classified into four groups, k = 1–2, 3–4, 5–7, and 8–15, each of which include more than 99 nuclei. For each group and each approach in consideration, we calculate the RMSD of extrapolated charge radii from the experimental data in the CR2013 database and plot them in Fig. 6. One sees, as expected, that the RMSD values of Eq. (4) and WS* models are smaller than those of other three models in all groups. We note that although the accuracies of the RCHB model are close to those of our empirical formula [Eq. (4)] and WS* models at k = 1–2, their RMSD values increase quickly for cases far from known borders. The RMSD values for overall predicted nuclei are summarized in Table III, from which one sees that the WS* models and Eq. (4) (RMSD values in bold font) present extrapolated charge radii with the smallest deviations in this numerical experiment.

TABLE III. RMSD (in unit of fm) of our extrapolated charge radii from the CR1999 database [49] or the CR2004 database [50] to the CR2013 database [10,11], by using the δR_k relations discussed in this paper. The results based on Eq. (4) and WS* model (which yield the smallest RMSD values) are presented in bold font.

Model	CR1999	CR2004
EMP [Eq. (4)]	**0.0124**	**0.0149**
HFB-31 [24]	0.0163	0.0175
RCHB [28]	0.0193	0.0149
RMF + BCS [26]	0.0263	0.0266
WS* [40]	**0.0133**	**0.0115**

Similarly, we perform the numerical experiment of extrapolation from the CR2004 database to the CR2013 database, and again the WS* model and Eq. (4) yield the smallest RMSD values for 133 nuclei, as seen in the third column of Table III. In this numerical experiment, major differences between predictions of the WS* model and those of Eq. (4) arise from the $N = 40$ subshell effect in Ga ($Z = 31$) isotopes [6], which lead to a sudden change (about 0.03 fm) of charge radius from ^{71}Ga to ^{73}Ga, and this sudden change is not included in Eq. (4). After we exclude the results of Ga isotopes, the RMSD values for the WS* model and Eq. (4) would be changed to 0.0121 and 0.0129 fm, respectively. Similarly, Eq. (4) should not be used for isotope chains from Ni ($Z = 28$) to Br ($Z = 35$), because the relevant δR_k suffer from the $N = 40$ subshell effect. We note that, without details, by using δR_{in-jp} relations, the RMSD values of extrapolations from the CR1999 and CR2004 database to the CR2013 database are 0.0151 and 0.0091 fm (for 353 and 85 nuclei) [45], respectively, excluding the regions discussed in Sec. II A.

In addition to the remarkable accuracy for extrapolation, as demonstrated above, another important advantage of the present approach is that the δR_k relations involve charge radii of only two nuclei, thus one is able to evaluate nuclear charge radius of a nucleus provided that the charge radius of one nucleus along the same isotope chain is accessible in principle. This is in contrast to extrapolations by using the δR_{in-jp} relations, which require additionally charge radii of two neighboring nuclei with proton number $Z + j$ or $Z - j$, and therefore the present approach is much more flexible in applications.

The remarkable predictive power of δR_k with the WS* model and Eq. (4) is encouraging, therefore we apply these two approaches, with k from 1 to 15, to predict charge radii starting from the CR2013 database. Our prediction of charge radii is restricted to nuclei with positive one- and two-neutron (proton) separation energies in the WS* database, and excludes anomalous regions pointed in Sec. II A. Two sets of predicted charge radii, denoted as R_{WS^*} and R_{emp}, are obtained by using δR relations of the WS* model and Eq. (4), respectively. We also obtain the average values of the two results for each nucleus, denoted by $R_{\mathrm{th}}(N, Z)$. We denote the uncertainties of these two predictions by σ_{WS^*} and σ_{emp}, and our theoretical uncertainty σ_{th} for $R_{\mathrm{th}}(N, Z)$ is defined by

$$\sigma_{\mathrm{th}} = \max\left[\frac{\sqrt{\sigma_{\mathrm{emp}}^2 + \sigma_{\mathrm{WS}*}^2}}{2}, \frac{|R_{\mathrm{emp}} - R_{\mathrm{WS}*}|}{2}\right]. \quad (10)$$

The first, square-root term on the right-hand side corresponds to statistic uncertainties, and the latter represents difference between these two evaluations, just like the value of uncertainty in Ref. [10].

In total we are able to predict charge radii of 1647 nuclei unaccessible in the CR2013 database, with theoretical uncertainty below 0.03 fm. We tabulate these predicted results, together with the CR2013 results, in the Supplemental Material [51] (note that we have replaced the decimal points with # for Re ($Z = 75$), Po ($Z = 84$), Rn ($Z = 86$), Fr ($Z = 87$), Ra ($Z = 88$), and Cm ($Z = 96$) isotopes, because the "experimental" data compiled in the CR2013 are actually based on a simple formula; see Eq. (8) in Ref. [10]). The nuclei whose charge radii are predicted by our extrapolations in this paper are shown in Fig. 7(a), where squares in black correspond to nuclei which are accessible in the CR2013 database, and squares in other colors correspond to nuclei whose radii uncertainties are predicted in this work based on Eq. (10). We also plot the nuclei whose charge radii are predicted in the Supplemental Material of Ref. [45], based on the δR_{in-jp} relations, in Fig. 7(b). One sees theoretical uncertainties of the δR_{in-jp} relations increase much more rapidly, as they extend from known borders of isotope chains, than the δR_k relations in this paper.

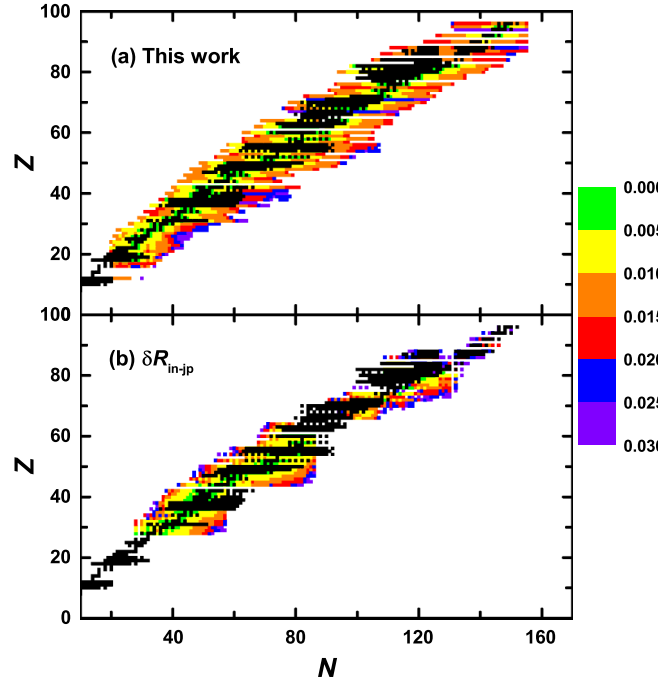

FIG. 7. Theoretical uncertainties (in units of fm) of our predicted charge radii. Panel (a) corresponds to predictions by using the δR_k relations and Eq. (10), and panel (b) corresponds to those predicted by the δR_{in-jp} relations [45]. Solid squares in black correspond to nuclei which are experimentally accessible in the CR2013 database [10,11]. One sees that the approach in this paper predicts many more charge radii than the δR_{in-jp} relations within given accuracy, 0.03 fm.

Recently, mean-squared charge-radii changes δR^2 [see its definition in Eq. (5)] of some nuclei in the K, Cu, Zn, Sn, and Hg isotope chains with respect to $^{39}_{19}$K$_{20}$, $^{65}_{29}$Cu$_{36}$, $^{68}_{30}$Zn$_{38}$, $^{124}_{50}$Sn$_{74}$, and $^{198}_{80}$Hg$_{118}$, respectively, have been experimentally measured or reevaluated by using laser spectroscopy techniques [13–20]. Here we use these results as the touchstone of our predicted results. For K isotopes a set of nuclear charge radii R were presented in Ref. [14], and for the other four isotope chains experimental values of δR^2 [see Eq. (5)] were presented with respect to ^{65}Cu, ^{68}Zn, ^{124}Sn, and ^{198}Hg, respectively [15–20]. In Fig. 8 we plot R and δR^2 by using solid and hollow up-triangles, down-triangles, left-triangles, right-triangles, diamonds, and stars, where the corresponding

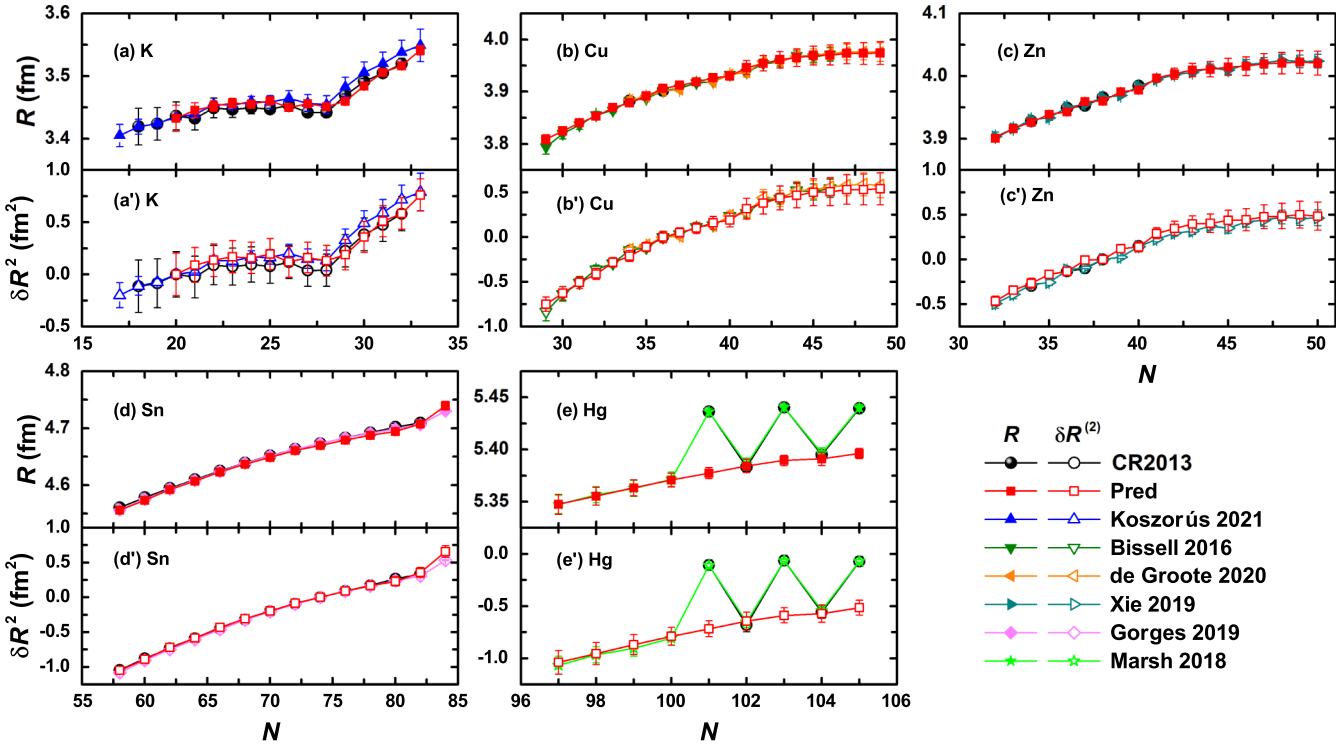

FIG. 8. Nuclear charge radii R and δR^2 extrapolated based on the CR2013 database, and selected experimental results published in 2016–2021. The results of the CR2013 database and our predicted results are plotted in black and red, respectively; and latest experimental results (unaccessible in the CR2013 database) taken from Refs. [14,16–20] are plotted in other colors. Panels (a)–(e) correspond to K ($Z = 19$), Cu ($Z = 29$), Zn ($Z = 30$), Sn ($Z = 30$), and Hg ($Z = 80$) isotopes, respectively.

predictions by using δR_k relations and Eq. (5) are denoted by solid and open squares in red, respectively. For convenience and completeness, we also plot the experimental data of these isotope chains of the CR2013 database by using circles in black. One sees that the evolution of our extrapolated results agrees very well with new experimental data, except for R and δR^2 of ^{181}Hg, ^{183}Hg, and ^{185}Hg, which belong to the "anomalous" region.

In Table IV we list the RMSD of our extrapolated R and $\delta R^{(2)}$ from these new experimental data. The RMSD values for R are 0.0121, 0.0042, and 0.0036 fm for K, Zn, and Sn, respectively. We should note that the RMSD for K isotope chain is relatively large, as the proton number of K is small. For Cu isotopes, the RMSD is 0.0056 fm with respect to results in Ref. [16] and it is 0.0049 fm with respect to results in [17]. This remarkable accuracy of prediction is very encouraging, because there are only two nuclear charge radii for ^{63}Cu and ^{65}Cu in the original CR2013 database, and with respect to these two results we are able to predict the charge radius of ^{78}Cu by using $\delta R_k^{(\mathrm{th})}$ for which $k = 13$. For Hg isotopes, the total RMSD for nine nuclei is 0.0298 fm, but with exclusion of ^{181}Hg, ^{183}Hg, and ^{185}Hg the RMSD is reduced dramatically to 0.0024 fm.

TABLE IV. RMSD of our predicted R (in units of fm) and δR^2 (in units of fm^2) from selected experimental results published in 2016–2021, for K, Cu, Zn, Sn and Hg isotopic chains. For convenience we also present RMSD values of the same set of data obtained by using the δR_{in-jp} relations of Ref. [45]. The results of ^{181}Hg, ^{183}Hg, and ^{185}Hg are excluded in calculating the RMSD values here.

	This work		δR_{in-jp} [45]	
Element	R	$\delta R^{(2)}$	R	$\delta R^{(2)}$
K [14]	0.0121	0.0769		
Cu [16]	0.0056	0.0385	0.0064	0.0509
Cu [17]	0.0049	0.0469	0.0068	0.0564
Zn [18]	0.0042	0.0538	0.0063	0.0539
Sn [19]	0.0036	0.0415	0.0023	0.0232
Hg [20]	0.0024	0.0244		

According to Table IV, the RMSD values of $\delta R^{(2)}$ are 0.0769 fm^2 for K; 0.0385 fm^2 for Cu with respect to results of Ref. [16] and 0.0469 fm^2 with respect to results fo Ref. [17]; 0.0538 fm^2 for Zn; 0.0415 fm^2 for Sn; and 0.0244 fm^2 for Hg isotopes (excluding ^{181}Hg, ^{183}Hg, and ^{185}Hg). The δR_{in-jp} relations are also evaluated with respect to the new experimental data of Cu, Zn, and Sn, as shown in the fourth and fifth columns of Table IV. Except for Sn isotopes, the δR_{in-jp} relations are less accurate than the δR_k relations presented in this paper.

IV. DISCUSSION AND CONCLUSIONS

To summarize, in this paper we study systematics of differences between nuclear charge radii of two nuclei with the same proton number, δR_k, and based on an empirical formula and a number of theoretical databases we predict charge radii

which are not yet experimentally accessible by simple extrapolations.

First, we have investigated the systematics of δR_1 (differences between charge radii of two neighboring isotopes) extracted from the CR2013 database, and suggest an empirical formula which describes the N dependence of δR_1, the resultant RMSD of which is 0.0050 fm, with exclusion of the light nuclei region ($N < 20$) and three regions relevant to phase transition and shape coexistence. We have also extracted δR_1 based on charge radii calculated by a number of theoretical models, including the HFB-31, RCHB, RMF + BCS, and WS* models. The δR_1 relations based on the RCHB and WS* models are found to be remarkably consistent with experimental data, with RMSD values of these two approaches being 0.0057 and 0.0066 fm, respectively, for the same set of databases as the empirical formula of δR_1 in this paper. As for simple relations of δR_k, the deviations of results extracted based on the RCHB calculations with respect to experimental data become large, while the empirical formula and results based on the WS* calculations remain very accurate.

Second, we study the predictive power of the δR_k relations by performing two numerical experiments, one of which is to extrapolate the results of the CR1999 and CR2004 database to those of the CR2013 database, and the other of which is to extrapolate the CR2013 database to the new experimental results of R and δR^2 measured in the last few years. The accuracies of our predictions based on the empirical formula and the WS* models are in general more accurate than results given by the δR_{in-jp} relations [45], with the virtue of simplicity and flexibility; and furthermore, the extrapolation of the δR_k approach is carried out without iteration and thus it avoids rapid accumulation of theoretical uncertainties in predictions.

Finally, our predicted nuclear charge radii by using δR_k based on our empirical formula and the WS* model, for those with theoretical uncertainty below 0.03 fm, are tabulated in the Supplemental Material of this paper [51]. These predictions are relevant to ongoing research programs at radioactive ion beam facilities, e.g., experimental measurements planned on both Zn [52] and Ag [53].

ACKNOWLEDGMENTS

We are grateful to B. H. Sun for the recommendation of theoretical models used in the evaluation. We thank the National Natural Science Foundation of China (Grants No. 11975151 and No. 11961141003) and MOE Key Lab for Particle Physics, Astrophysics and Cosmology for financial support.

[1] I. Angeli, Y. P. Gangrsky, K. P. Marinova, I. N. Boboshin, S. Y. Komarov, B. S. Ishkhanov, and V. V. Varlamov, J. Phys. G **36**, 085102 (2009).
[2] K. T. Flanagan, K. M. Lynch, J. Billowes, M. L. Bissell, I. Budinčević, T. E. Cocolios, R. P. de Groote, S. De Schepper, V. N. Fedosseev, S. Franchoo, R. F. Garcia Ruiz, H. Heylen, B. A. Marsh, G. Neyens, T. J. Procter, R. E. Rossel, S. Rothe, I. Strashnov, H. H. Stroke, and K. D. A. Wendt, Phys. Rev. Lett. **111**, 212501 (2013).
[3] W. Nörtershäuser, D. Tiedemann, M. Žáková, Z. Andjelkovic, K. Blaum, M. L. Bissell, R. Cazan, G. W. F. Drake, C. Geppert, M. Kowalska, J. Krämer, A. Krieger, R. Neugart, R. Sánchez, F. Schmidt-Kaler, Z.-C. Yan, D. T. Yordanov, and C. Zimmermann, Phys. Rev. Lett. **102**, 062503 (2009).
[4] I. Budinčević, J. Billowes, M. L. Bissell, T. E. Cocolios, R. P. de Groote, S. De Schepper, V. N. Fedosseev, K. T. Flanagan, S. Franchoo, R. F. Garcia Ruiz, H. Heylen, K. M. Lynch, B. A. Marsh, G. Neyens, T. J. Procter, R. E. Rossel, S. Rothe, I. Strashnov, H. H. Stroke, and K. D. A. Wendt, Phys. Rev. C **90**, 014317 (2014).
[5] M. D. Seliverstov, T. E. Cocolios, W. Dexters, A. N. Andreyev, S. Antalic, A. E. Barzakh, B. Bastin, J. Büscher, I. G. Darby, D. V. Fedorov *et al.*, Phys. Lett. B **719**, 362 (2013).
[6] P. Campbell, I. D. Moore, and M. R. Pearson, Prog. Part. Nucl. Phys. **86**, 127 (2016).
[7] A. Ozawa, T. Suzuki, and I. Tanihata, Nucl. Phys. A **693**, 32 (2001).
[8] B. Cheal and K. T. Flanagan, J. Phys. G **37**, 113101 (2010).
[9] K. Blaum, J. Dilling, and W. Nörtershäuser, Phys. Scr. **2013**, 014017 (2013).
[10] I. Angeli and K. P. Marinova, At. Data Nucl. Data Tables **99**, 69 (2013).
[11] K. P. Marinova and I. Angeli, https://www-nds.iaea.org/radii/.
[12] A. Antognini, N. Berger, T. E. Cocolios, R. Dressler, R. Eichler, A. Eggenberger, P. Indelicato, K. Jungmann, C. H. Keitel, K. Kirch, A. Knecht, N. Michel, J. Nuber, N. S. Oreshkina, A. Ouf, A. Papa, R. Pohl, M. Pospelov, E. Rapisarda, N. Ritjoho, S. Roccia, N. Severijns, A. Skawran, S. M. Vogiatzi, F. Wauters, and L. Willmann, Phys. Rev. C **101**, 054313 (2020).
[13] Á. Koszorús, X. F. Yang, J. Billowes *et al.*, Phys. Rev. C **100**, 034304 (2019).
[14] Á. Koszorús, X. F. Yang, W. G. Jiang *et al.*, Nat. Phys. **17**, 439 (2021).
[15] A. J. Miller, K. Minamisono, A. Klose *et al.*, Nat. Phys. **15**, 432 (2019).
[16] M. L. Bissell, T. Carette, K. T. Flanagan *et al.*, Phys. Rev. C **93**, 064318 (2016).
[17] R. P. de Groote, J. Billowes, C. L. Binnersley *et al.*, Nat. Phys. **16**, 620 (2020).
[18] L. Xie, X. F. Yang, C. Wraith *et al.*, Phys. Lett. B **797**, 134805 (2019).
[19] C. Gorges, L. V. Rodríguez, D. L. Balabanski *et al.*, Phys. Rev. Lett. **122**, 192502 (2019).
[20] B. A. Marsh, T. Day Goodacre, S. Sels *et al.*, Nat. Phys. **14**, 1163 (2018).
[21] S. Sels, T. Day Goodacre, B. A. Marsh *et al.*, Phys. Rev. C **99**, 044306 (2019).
[22] M. V. Stoitsov, J. Dobaczewski, W. Nazarewicz, S. Pittel, and D. J. Dean, Phys. Rev. C **68**, 054312 (2003), and references therein.
[23] S. Goriely, N. Chamel, and J. M. Pearson, Phys. Rev. C **82**, 035804 (2010).
[24] S. Goriely, N. Chamel, and J. M. Pearson, Phys. Rev. C **93**, 034337 (2016).

[25] G. A. Lalazissis, S. Raman, and P. Ring, At. Data Nucl. Data Tables **71**, 1 (1999).
[26] L. S. Geng, H. Toki, and J. Meng, Prog. Theor. Phys. **113**, 785 (2005).
[27] P. W. Zhao, Z. P. Li, J. M. Yao, and J. Meng, Phys. Rev. C **82**, 054319 (2010).
[28] X. W. Xia, Y. Lim, P. W. Zhao *et al.*, At. Data Nucl. Data Tables **121–122**, 1 (2018).
[29] F. Buchinger, J. E. Crawford, A. K. Dutta, J. M. Pearson, and F. Tondeur, Phys. Rev. C **49**, 1402 (1994).
[30] F. Buchinger, J. M. Pearson, and S. Goriely, Phys. Rev. C **64**, 067303 (2001).
[31] F. Buchinger and J. M. Pearson, Phys. Rev. C **72**, 057305 (2005).
[32] H. Iimura and F. Buchinger, Phys. Rev. C **76**, 057302 (2007).
[33] H. Iimura and F. Buchinger, Phys. Rev. C **78**, 067301 (2008).
[34] J. Y. Zeng, Acta Phys. Sinica **13**(5), 357 (1957).
[35] J. Y. Zeng, Acta Phys. Sinica **24**(2), 151 (1975).
[36] B. Nerlo-Pomorska and K. Pomorski, Z. Phys. A **348**, 169 (1994).
[37] S. Q. Zhang, J. Meng, S.-G. Zhou, and J. Y. Zeng, Eur. Phys. J. A **13**, 285 (2002).
[38] J. Duflo, Nucl. Phys. A **576**, 29 (1994).
[39] A. E. L. Dieperink and P. Van Isacker, Eur. Phys. J. A **42**, 269 (2009).
[40] N. Wang and T. Li, Phys. Rev. C **88**, 011301(R) (2013).
[41] J. Piekarewicz, M. Centelles, X. Roca-Maza, and X. Viñas, Eur. Phys. J. A **46**, 379 (2010).
[42] B. H. Sun, Y. Lu, J. P. Peng, C. Y. Liu, and Y. M. Zhao, Phys. Rev. C **90**, 054318 (2014).
[43] B. H. Sun, C. Y. Liu, and H. X. Wang, Phys. Rev. C **95**, 014307 (2017).
[44] M. Bao, Y. Lu, Y. M. Zhao, and A. Arima, Phys. Rev. C **94**, 064315 (2016).
[45] M. Bao, Y. Y. Zong, Y. M. Zhao, and A. Arima, Phys. Rev. C **102**, 014306 (2020).
[46] I. O. Morales and A. Frank, Phys. Rev. C **83**, 054309 (2011).
[47] G. J. Fu, Y. Lei, H. Jiang, Y. M. Zhao, B. Sun, and A. Arima, Phys. Rev. C **84**, 034311 (2011).
[48] V. Manea, P. Ascher, D. Atanasov *et al.*, Phys. Rev. C **95**, 054322 (2017).
[49] I. Angeli, Table of nuclear root mean square charge radii, INDC(HUN)-033, IAEA Nuclear Data Section, Vienna, 1999.
[50] I. Angeli, At. Data Nucl. Data Tables **87**, 185 (2004).
[51] See Supplemental Material at http://link.aps.org/supplemental/10.1103/PhysRevC.104.014303 for the predicted charge radii of nuclei with neutron number $N \geqslant 20$.
[52] X. F. Yang, T. E. Cocolios, and S. Geldhof, https://cds.cern.ch/record/2731961?ln=en
[53] R. P. de Groote, http://cds.cern.ch/record/2717869/?ln=en.